Estimation of Cooling Rates During Close-Coupled Gas Atomization using Secondary Dendrite Arm Spacing Measurement

Andrew M. Mullis, Leane Farrell and Robert F Cochrane
Institute for Materials Research
University of Leeds
Leeds LS2-9JT, UK

Nicholas J. Adkins
IRC in Materials Processing,
The University of Birmingham
Edgbaston
Birmingham B15-2TT, UK

ABSTRACT

Al-4 wt.%Cu alloy has been gas atomized using a commercial close-coupled gas atomization system. The resulting metal powders have been sieved into six size fractions and the secondary dendrite arm spacing has been determined using electron microscopy. Cooling rates for the powders have been estimated using a range of published conversion factors for Al-Cu alloy, with reasonable agreement being found between sources. We find that cooling rates are very low compared to those often quoted for gas atomized powders, of the order of 10^4 K s^{-1} for sub-38 μm powders. We believe that a number of numerical studies of gas atomization have overestimated the cooling rate during solidification, probably as a consequence of overestimating the differential velocity between the gas and the particles. From the cooling rates measure here we estimate that such velocities are unlikely to exceed 20 m s^{-1}.

1 Introduction

Close-coupled gas atomization (CCGA) is an important technique for the commercial production of fine, spherical metal powders. Such powders have a variety of uses, such as for pigments, catalysts, metal injection moulding (MIM) feedstock, solder pastes for 'flip-chip' type circuit board fabrication and solid rocket propellant. One of the advantages of gas atomized powders over conventionally cast materials is the high cooling rates experienced by the metal during solidification in flight [1, 2]. This leads to many desirable properties including a decrease in segregation, higher solid solubility and a finer microstructure which in turn gives better chemical homogeneity, a more corrosion resistant end product and more favourable hot and cold working properties. Moreover, high cooling rates and the sub-division of the melt into fine droplets can also give rise to significant undercooling in the melt [3], allowing access to metastable phases that under close to equilibrium processing conditions would be inaccessible.

Despite the importance of rapid cooling to the performance of gas atomized metal powders the range of cooling rates quoted for these varies considerably. At the lower end of this spectrum Zeoli et al. [4] and Shulka et al. [5] quote $10^2 - 10^4$ K s^{-1} while much higher rates of $10^5 - 10^8$ K s^{-1} are quoted by He et al. [6] and intermediate values up to 10^5 K s^{-1} are given by Kearns [2] and by Kellie [7]. In part these differences may be explained by the fact that the values are quoted for a range of

different particles sizes, atomization pressures, atomizing gases (including air, Argon and Helium) and atomizer configurations. However, this cannot account for all of the discrepancy, suggesting there is still considerable uncertainty regarding the cooling rates that may be encountered during the gas atomization of liquid metals.

Estimates of the cooling rate during gas atomization are generally made either on the basis of theoretical models [4, 6] or by measuring the secondary dendrite arm spacing in the resulting powder product [5]. The starting point for modelling the cooling rate is the balance of heat fluxes for a given droplet, which can be expressed as

$$\frac{dT_p}{dt}\left[c_l(1-f)+c_s f - L\frac{df}{dt}\right] = \frac{6h}{\rho d}(T_p - T_g) + \frac{6\varepsilon\sigma_b}{\rho d}(T_p^4 - T_R^4) \tag{1}$$

where T_p is the instantaneous temperature of the particle, c_l and c_s are the specific heat of the metal in the liquid and solid states respectively, f is the solid fraction, h the heat transfer coefficient, ρ the density of the metal, d the diameter of the droplet, ε the emissivity of the droplet surface, σ_b the Stefan-Boltzman constant, T_g the temperature of the gas and T_R the effective radiative temperature of the environment of the particle.

Shulka *et al*. [5] have used such a model combined with classical heterogeneous nucleation theory to estimate the cooling rate and undercooling of droplets within an atomization spray as a function of their diameter. They used an empirical model for the convective heat transfer coefficient, h, given by [8] as

$$h = \frac{\kappa_g}{d}\left(1 + 0.3\sqrt{\mathrm{Re}}\sqrt[3]{\mathrm{Pr}}\right) \tag{2}$$

where κ_g is the thermal conductivity of the gas and Re and Pr are the Reynolds and Prandtl numbers for the flow given by

$$\mathrm{Pr} = \frac{c_{pg}\mu}{\kappa_g} \quad , \qquad \mathrm{Re} = \frac{\rho_g d}{\mu}\left|v_p - v_g\right| \tag{3}$$

where c_{pg} is the specific heat capacity of the gas, μ is its kinematic viscosity and $\left|v_p\text{-}v_g\right|$ is the differential velocity between the particle and the gas.

Shulka *et al*. [5] estimated that cooling rates for 40 μm particles could approach 7×10^4 K s^{-1}, although this did not appear to agree well with their own experimental data. A broadly similar model was presented by He *et al*. [6] for the atomization of Al-Ni-Ce-Fe-Cu bulk amorphous alloy, wherein they estimated that cooling rates for 40 μm particles could approach 10^5 K s^{-1} for atomization in Ar and 10^6 K s^{-1} for atomization in He. Zeoli *et al*. [4] have used a computational fluid dynamics model of the atomization process to estimate h in a more rigorous manner, but their analysis is rather restricted by the large size of the particles (1-5 mm) they introduced as tracers into the gas.

Experimental techniques for determining cooling rates in as-solidified materials are based around the measurement of secondary dendrite arm spacing (SDAS). Unlike

most other solidification length scales, such as primary dendrite spacing and eutectic spacing, secondary dendrite arm spacing is determined not during the initial growth of the solid from the liquid, but by coarsening during the period in which the solid and liquid co-exist in the mushy zone [9, 10]. As such, SDAS can potentially be a sensitive measure of the post-recalescence cooling rate.

Theoretically, the process is well understood, with thinner secondary arms melting back from their tips and eventually disappearing due to their higher curvature, thereby increasing the spacing between adjacent arms [11, 12]. Experimentally, this gives rise to an expression for the SDAS, λ, which is given by [13] as,

$$\lambda = \lambda_0 R^{-n} \tag{4}$$

where R is the cooling rate, λ_0 is a constant and the exponent n is in the range 0.2-0.4. However, there has been little application of the technique to gas atomized powders. Shukla *et al.* [5] have used the measurement of SDAS in gas atomized Al-Cu powders to compare against theoretically calculated cooling curves, finding that the latter overestimated the cooling rate by a factor of around 3. However, as the main purpose of their paper was to present their theoretical model, little detail was given on the how the experimental results were obtained.

In this paper we use the measurement of secondary dendrite arm spacing to estimate the cooling rate of Al-Cu powders produced by a commercial gas atomizer, with an analysis of the uncertainties inherent in both the measurement of the secondary arm spacing and the subsequent conversion from SDAS to cooling rate. The correlation between SDAS and cooling rate in Al-Cu alloy at the Al-rich end of the phase diagram has been widely studied and consequently a number of conversions from SDAS are available [14, 15, 16, 17, 18]. The effect on the estimated cooling rate of applying these various scaling laws is considered fully in the Section 3.

2 Experimental Methods

Powders of the alloy Al-4wt.% Cu were produced by close-coupled gas atomization. The atomizer utilises a simple die of the discrete jet type with 18 cylindrical jets of 0.5 mm diameter arranged around a tapered melt delivery nozzle at an apex angle of 45°. The design, which is shown schematically in Fig. 1, is similar to the USAG [19] and Ames HPGA-I [20] designs. Although these designs are known to be sub-optimal in their atomization performance, the cylindrical jets giving rise to choked flow which limits the outlet gas velocity to Mach 1, we have used this geometry as it has been discussed extensively in the literature.

The liquid metal is delivered to the tip of the atomization nozzle via a central 2 mm diameter bore, wherein it wets the tip of the nozzle and is stripped off the circumferential edge. In order to ensure the smooth flow of liquid metal an over pressure of 40 kPa is applied to the reservoir above the atomization nozzle. In order to prevent oxidation of the liquid metal Ar was used as the atomizing gas. The atomization pressure was 3.5 MPa, giving a gas flow rate of 0.049 kg s^{-1}. The melt pour temperature was 1620 K. The atomization conditions were chosen so as to mimic those used in a broad range of commercial powder production scenarios.
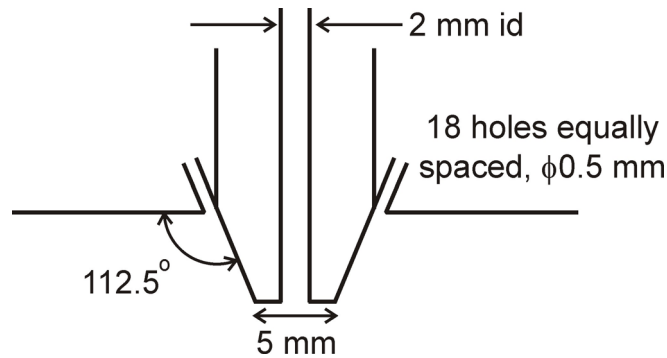
Fig. 1. Schematic diagram of the atomizer nozzle configuration.

Following atomization the powder was sieved into 6 size ranges, as given in Table 1, on the working assumption that particles of smaller diameter will cool more rapidly than those of larger diameter and that this will consequently give rise to a smaller secondary dendrite arm spacing. Samples of each size fraction were subsequently hot mounted in transcopic resin and polished flat for SEM analysis using a LEO 1530 Gemini FEGSEM.

Table 1 – Sieve size ranges used for powder classification

Particle diameter range
150 μm < d ≤ 212 μm
106 μm < d ≤ 150 μm
75 μm < d ≤ 106 μm
53 μm < d ≤ 75 μm
38 μm < d ≤ 53 μm
d ≤ 38 μm

In order to determine the best approach for measuring the secondary dendrite arm spacing imaging has been conducted using both backscatter electron (BSE) detection (atomic number contrast) on samples polished to a flat surface and secondary electron (SE) detection (topographic contrast) on samples polished flat and then etched for 20 s using Keller's reagent (2.5% nitric acid, 1.5% hydrochloric acid, 1% hydrofluoric acid, balance distilled water). A comparison of the images obtained using the two techniques is shown in Fig. 2. In both cases images are formed due to the interdendritic channels being enriched in Cu as a consequence of partitioning during solidification. The images show relatively fine, Cu rich, interdendritic channels separated by much broader secondary dendrite arms. This interpretation is confirmed in the EDX maps shown in Fig. 3 which show that the broad secondary dendrite arms are Cu deficient while the fine interdendritic channels are Cu enriched.

It is clear from Fig. 2 that both imaging techniques produce images from which measurements of secondary dendrite arms spacing can be made, but in general we find that the images from the SE imaging of etched samples are clearer and it is from these images that measurements have been made. Such measurements can be made either by measuring between the centres of adjacent secondary arms or, equivalently,

by measuring between adjacent interdendritic channels. However, as the error associated with identifying the centres of the interdendritic channels is less than that associated with identifying the centres of the secondary arms, the latter of these two approaches has been adopted.
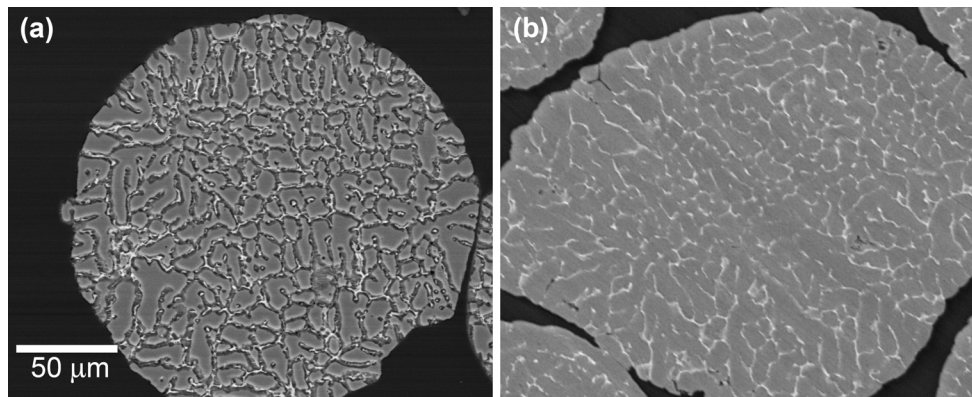

Fig. 2. Example electron images of Al-4 wt.%Cu droplets imaged by (a) secondary electron imaging on an etched sample and (b) backscatter electron imaging of an unetched sample.
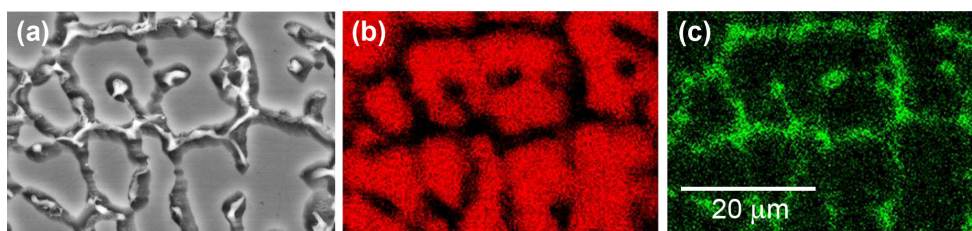

Fig. 3. Secondary electron image (a) and EDX maps (b & c) showing Al rich secondary dendrite arms (b) and Cu rich interdendritic channels (c).

3 Results

3.1 Secondary Dendrite Arm Spacing

For each of the six size fractions secondary dendrite arm spacings were measured from at least 10 different particles with a minimum of 100 measurements being made in total. The relative cumulative frequency plot for one size fraction (212-150 μm) is shown in Fig. 4. Plots for the other size fractions were broadly similar in shape but are not reproduced here for the sake of brevity. The mean SDAS for the six size fractions is plotted as a function of the mean size within the fraction in Fig. 5. The plot indicates that to a reasonable approximation the SDAS decreases linearly with mean particle size from 7.41 μm in the 212-150 μm sieve fraction to 2.08 μm in the < 38 μm sieve fraction.

Error bars are shown in the plot and represent ± 1σ, with σ being the sample standard deviation, which has been calculated for the data within each size fraction. This variation will reflect the cumulative effect of our measurement errors in determining the SDAS, the statistical variability in making measurements on an inherently stochastic process such as coarsening and variations due to different diameter particles within each size fraction experiencing different cooling rates.
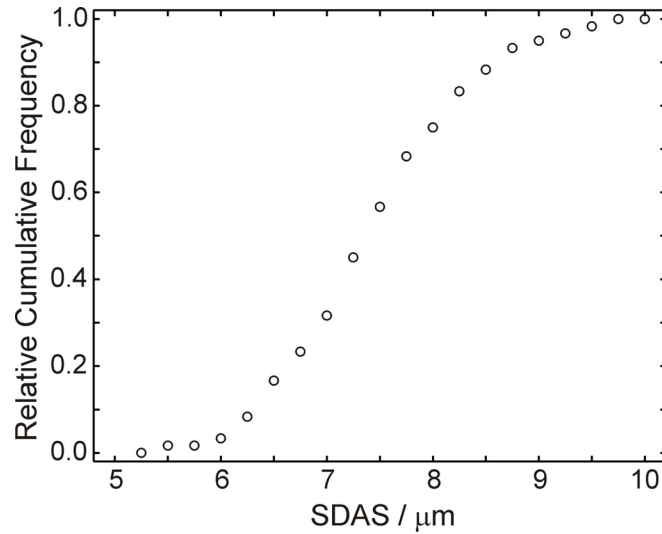
Fig. 4. Relative cumulative frequency for the measured secondary dendrite arm spacing in the 212-150 μm size fraction.
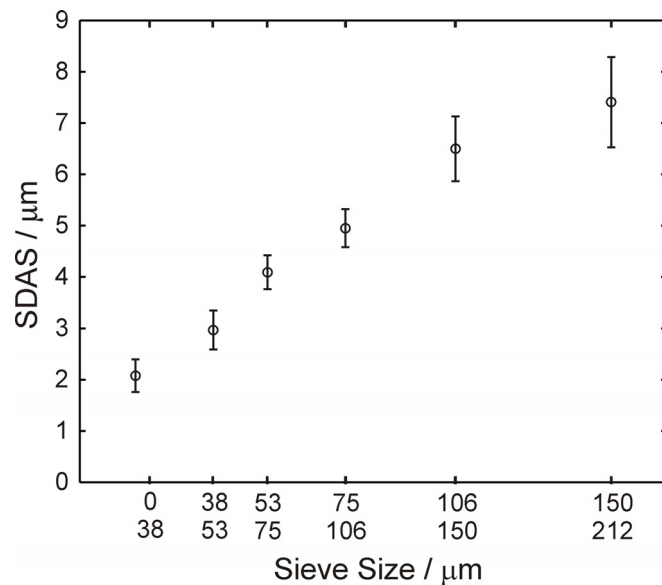

Fig. 5. Mean secondary dendrite arm spacing as a function of sieve size. Error bars are ± 1 standard deviation, in each case estimated from that size fraction.

3.2 Conversion to Cooling Rate

A number of studies have attempted to obtain empirical relationships of the form given by Equ. (4) to relate secondary dendrite arm spacing to cooling rate in hypo-eutectic Al-Cu alloys. Generally, such relationships are obtained by measuring the SDAS for samples which have either been directionally solidified in a linear temperature gradient furnace [14, 15], or by casting into a wedge shaped mould [16, 17]. In the former case the product of the temperature gradient (K m^{-1}) and pulling speed (m s^{-1}) gives the cooling rate experienced by sample (K s^{-1}). In this work we do not consider the results obtained in [16], as their alloy was based on a commercial

A206 composition and therefore also contained Si, Fe, Mn, Mg and Ti in addition to Al and Cu, the presence of which may seriously affect the coarsening behaviour of the dendrite arms.

A number of difficulties are encountered when attempting to apply relationships obtained from a linear temperature gradient furnace to estimate cooling rates pertaining to rapid solidification processes such as gas atomization. In order to obtain accurate cooling rates when using a linear temperature gradient furnace the pulling speed must be sufficiently slow so as to ensure that all heat transfer is along the axial temperature gradient and that no radial temperature gradients are established. This generally limits the pulling speed to < 0.002 m s^{-1} and the corresponding solidification cooling rate to $O(10$ K s$^{-1})$. However, when these are then applied to process such as gas atomization the cooling rates are likely to be 2-4 orders of magnitude higher, wherein significant uncertainty can be introduced as small errors in the exponent, n, can produce large errors in the extrapolated cooling rate. Moreover, there is a further complication as various authors have tended to work on similar, but not identical, compositions and, as pointed out by Eskin et $al.$ [17], the pre-exponential factor λ_0 is dependant upon the Cu concentration of the alloy, with higher Cu concentrations giving finer secondary dendrite arm spacings. Nonetheless, this is probably the best technique available to estimate solidification cooling rates from as-solidified samples and in this work we use a variety of sources to establish the extent to which agreement can be obtained.

One of the first comprehensive investigations of SDAS in Al-Cu alloys was presented by Horwath & Mondolfo [14] who studied 8 different Cu concentrations, with the closest to that studied here being 5.0 wt.% Cu, and at cooling rates of < 1 K s^{-1} to ≈ 20 K s^{-1}. They give the secondary dendrite arm spacing (reproduced here verbatim) as

$$\lambda = A \exp B \ln R + CM \tag{5}$$

where A, B, C are constants and M is the alloy concentration. Unfortunately, the form of Equ. (5) above is ambiguous and, moreover, for the constants given by [14] we have been unable, for any reasonable interpretation of Equ. (5), to reconstruct the raw data from which they claim to have derived the relationship. We have therefore used their raw data to fit a relationship of the form of Equ. (4), wherein for a 4 wt.% Cu alloy we obtain $\lambda_0 = 43.4$ μm and $n = 0.32$.

Data for secondary dendrite arm spacing in Al-Cu and Al-Si alloys obtained from a linear temperature gradient furnace is also given by Sarreal & Abbaschian [15]. For Al-Cu they use a single alloy of composition 4.9 wt.% Cu but cover a wider range of cooling rates, up to a 187 K s^{-1}. They give $\lambda_0 = 46.6$ μm and $n = 0.29$.

Eskin et $al.$ [17] have used the mould cooling technique to study secondary dendrite arm spacing for 6 different alloy compositions, of which 4.3 wt.% Cu is the closest to the one used in this study. Cooling rates are generally in the range 0.2-12 K s^{-1} and have been determined via thermocouples inserted in the mould. In their analysis Eskin et $al.$ quote two cooling rates for each experiment performed, a total cooling rate, which is the liquidus-solidus temperature range divided by the total time taken for solidification, and the linear cooling rate obtained from the linear section of the

cooling curve between the liquidus and solidus temperatures, which they consider to be superior. They consequently arrive at two different sets of coefficients for each composition. Interpolated to the 4 wt.% Cu composition used here these would be $\lambda_0 = 77.1$ μm and $n = 0.40$ for the total cooling rate and $\lambda_0 = 87.2$ μm and $n = 0.41$ for the linear cooling rate.

A comprehensive analysis of the secondary dendrite arms spacing in Al-4wt.% Cu has been given by Kasperovich *et al.* [18] covering cooling rates between 0.01 K s^{-1} and 14,000 K s^{-1}. As no one solidification technique is amenable to producing such a wide range of cooling rates, samples solidified by four separate technique were analysed. For cooling rates up to 0.36 K s^{-1} samples were solidified in the ARTEMIS [21] linear gradient furnace, casting into an aerogel mould was used to produces samples with cooling rates in the range 0.98 - 232 K s^{-1}, while an 8.5 m drop-tube was used to access cooling rates between 155 K s^{-1} and 14,070 K s^{-1}. In addition one data point was obtained from an electromagnetically levitated sample where the cooling rate was measured directly at 2.9 K s^{-1} using a 2-colour pyrometer. Kasperovich *et al.* fit their combined data set with a power law with $\lambda_0 = 54.5$ μm and $n = 0.328$. However, for their drop-tube samples [18] were unable to measure cooling rates directly, instead using a heat balance model similar to that defined by Equations (1-2) to estimate the cooling rate. In terms of the current study this would introduce an unacceptable circularity to the methodology if we were to use data reliant on Equations (1-2) as part of the calibration from which we will then measure cooling rates to assess the extent to which Equations (1-2) can be applied to gas atomization. For this reason we have omitted the drop-tube data from the fitting. This however also highlights that there is a systematic difference in the cooling rate-SDAS data between the ARTEMIS and EM levitation data on the one hand and the mould data of [18] on the other hand. We have therefore re-calculated the fitting parameters on the basis of the ARTEMIS and EM levitation data, obtaining $\lambda_0 = 54.8$ μm and $n = 0.339$. We note however that these are not very different to the combined value given by [18]. The data from all the sources used here is summarised in Table 2.

Table 2 – Parameters for the cooling rate models used in the work

R_{min} /K s^{-1}	R_{max} /K s^{-1}	Compositions	As calculated from source		Interpolated to 4 wt.% Cu		Source
			λ_0/μm	n	λ_0/μm	n	
0.014	0.56	8 (5.0 wt.%)			43.4	0.32	14
0.10	187	1 (4.9 wt.%)	46.6	0.29			15
0.20	9	6 (4.3 wt.%)	76.1	0.40	77.1	0.40	17 Total
0.30	12	6 (4.3 wt.%)	85.6	0.41	87.2	0.41	17 Linear
0.03	2.9	1 (4.0 wt.%)	58.7	0.355			18

The calculated cooling rates for the five conversion relationships quoted above are plotted in Fig. 6 as a function of secondary dendrite arm spacing, for the range of spacings typical of the droplets studied here (2 – 7.5 μm). From the figure it is clear that there is a reasonable level of agreement between the relationships due to Kasperovich *et al.* [18], Eskin *et al.* [17] (both linear and total cooling rate) and Horwath & Mondolfo [14], but that the relationship given by Sarreal & Abbaschian [15] yields cooling rates that are considerably in excess of the others. However,

noting that the maximum cooling rates given by Sarreal & Abbaschian [15] are significantly in excess of those quoted by the other authors we have reanalysed their data. They use a linear temperature gradient furnace and in order to achieve the high cooling rates quoted have used a combination of both high temperature gradients, 18700 K m^{-1}, and high pulling speeds, up to 0.1 m s^{-1}. However, the authors note that both primary and secondary dendrite arms were only distinguishable for pulling speeds of 0.0015 m s^{-1} or below (corresponding to cooling rates of ≤ 11.25 K s^{-1}). Moreover, at these high pulling speeds it is likely that radial temperature gradients will be established, wherein the cooling rate is no longer given by the product of temperature gradient and pulling speed. Due to these additional uncertainties in the data of [15] we have restrict the power law fit to data where the cooling rate is ≤ 11.25 K s^{-1}, wherein we obtain revised coefficients of $\lambda_0 = 47.5$ μm and $n = 0.3256$. The effect of this change is also shown on Fig. 6 by the line marked as 'Modified Sarreal & Abbaschian', from which it is apparent that much improved agreement with the other cooling rate estimates is obtained.
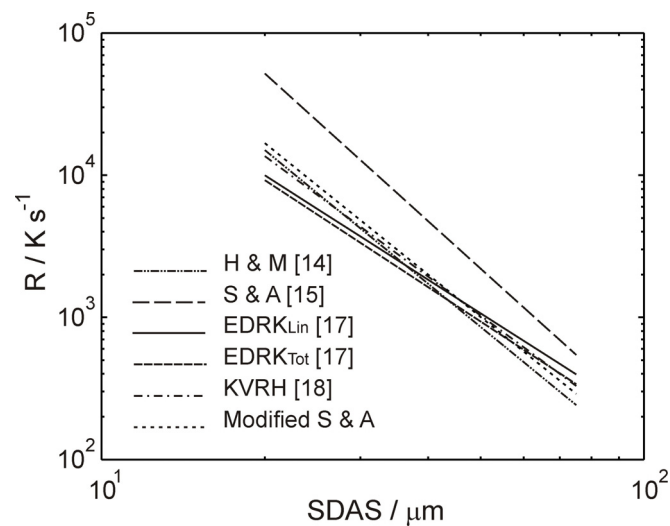

Fig. 6. Estimated cooling rate as a function of secondary dendrite arm spacing based on the relationships given by Horwath & Mondolfo (H & M) [14], Eskin *et al*. (EDRK) [17] (both linear and total cooling rate), Kasperovich *et al*. (KVRH) [18] and Sarreal & Abbaschian (S & A) [15]. The modified Sarreal & Abbaschian relationship is based on our refitting of their data excluding points with cooling rates in excess of 11.25 K s^{-1}.

The estimated cooling rate as a function of mean droplet size, based on the measured SDAS for the six size fractions studied, is given in Fig. 7 for each of the cooling rate models and a summary of the cooling rate data is given in Fig 8. In Fig. 8 the mean cooling rate for each sieve size is obtained from the geometric mean of the estimates based on the relationships given by Horwath & Mondolfo [14], Eskin *et al*. [17] (both linear and total cooling rate), Kasperovich *et al*. [18] and the modified relationship based on the data of Sarreal & Abbaschian [15]. Upper error estimates are based upon which ever of the five relationships gives the highest cooling rate for an SDAS of 1 standard deviation smaller than the mean while lower error estimates are based upon which ever of the five relationships gives the lowest cooling rate for an SDAS of 1 standard deviation larger than the mean. The resulting error bars therefore include the

effects of both the variation of SDAS within our sieve size fractions and the effect of the different cooling rate conversion factors. Mean cooling rates vary from ≈ 320 K s^{-1} for the 212-150 μm fraction to 11000 K s^{-1} for the < 38 μm size fraction. The data can be approximated reasonably well by a power law relationship wherein

$$(R / \mathrm{K\,s^{-1}}) = 1.87 \times 10^{6} (d / \mathrm{\mu m})^{-1.67} \qquad (6)$$

This is equivalent to fitting the SDAS date for the six sieve fractions with a power law of the form of Equ. (4) with the coefficients $\lambda_0 = 58.7$ μm and $n = 0.355$.
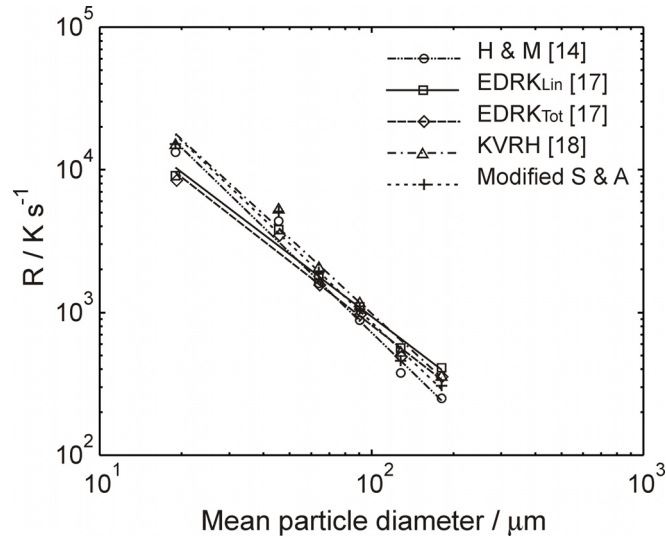

Fig. 7. Estimated cooling rate as a function of mean particle diameter based on the relationships given in Fig. 6.
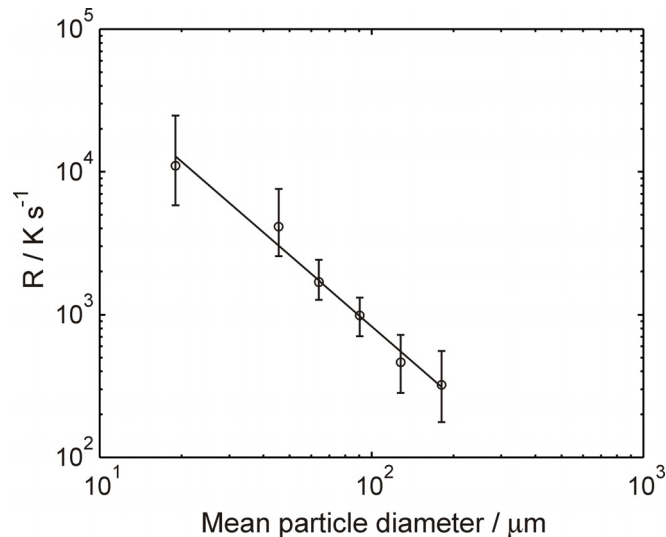

Fig. 8. Best estimate of the cooling rate as a function of mean particle diameter based upon measurement of secondary dendrite arm spacing. Error bars represent the cumulative uncertainty due to both variation in the SDAS within each size fraction (± 1 standard deviation) and variability in the different relationships between SDAS and cooling rate.

4 Discussion

The cooling rates reported in Fig. 7-8 are very much towards the low end of the spectrum of what would be expected for gas atomized powders and are very much lower than some estimates based upon numerical simulation. There are however many uncertainties which can potentially make the numerical estimation of atomization cooling rates unreliable. Both the gas temperature and the local radiative equilibrium temperature will depend upon the total heat input into the system, which in turn is determined by the melt temperature and flow rate. The gas temperature will also depend upon the rate of heat transfer from the droplets to the gas, i.e. there is an implicit coupling within the equation between T_g and dT_p/dt. In most numerical cooling rate models this has been ignored, indeed T_g and T_R are often taken as being close to ambient temperature, which is unlikely to be correct. However, the largest uncertainties are likely to be related to the heat transfer coefficient, estimation of which requires a knowledge of the relative velocity between the particle and the gas, via Re. In practice the complex interaction between the high velocity gas jets and the metal results in a turbulent, and often chaotic, flow with the result that the details of the flow are far from well understood. In particular, high speed imaging studies of the gas atomization process have revealed that atomizers are subject to quasi-periodic fluctuations on time scales from $0.1\text{-}10^{-3}$ s [22, 23], while the application of Particle Image Velocimetry (PIV) techniques to gas atomization [24] has revealed complex recirculation patterns both within the melt plume and in the adjacent gas. Moreover, due to the complexity of the process details of the flow have generally not been well captured by models of the atomization process. Even in the restricted number of cases where attempts have been made to capture the two phase interaction, these have generally used particles of fixed size (i.e. droplet breakup is ignored) [25, 26], a very small number of particles [4], or have been restricted to very small times after the second fluid is introduced due to the computationally intensive nature of the calculation [27]. Consequently, we believe that numerical atomization models may have significantly overestimated cooling rates.

The low cooling rates observed in this work would tend to be confirmed by comparison with the drop-tube data from [18]. In that work secondary dendrite arm spacings < 3 µm were observed for particles of diameter ≤ 137.8 µm. Conversely, in this work such small SDAS measurements were made only in the 53 - 38 µm and < 38 µm sieve fractions. We conjecture that much higher cooling rates were achieved in the drop-tube study due to the lower heat input to the system from the molten metal. In drop-tube studies the total sample volume is typically no more than a few grams, whereas several kilograms of melt will be processed over 1-2 minutes by even a small batch type gas atomizer as used in this study.

In order to assess the implications of the observed cooling rates on our understanding of the gas dynamics during atomization we have used Equations (1-2) to calculate the differential velocity between the particles and the gas which is required to give the observed cooling rates as a function of particle diameter. This is therefore the opposite of the normal modelling approach in which assumed or calculated flow velocities are used to estimate the expected cooling rate. The parameters used in the model are given in Table 3.

Table 3 – Parameters used to relate cooling rate to differential velocity

Quantity	Value	Units
Properties of the gas		
Specific heat, c_{pg}	521.62	J kg^{-1} K^{-1}
Density, ρ_g	1.6617	kg m^{-3}
Kinematic viscosity, μ	1.3416×10^{-5}	m^2 s^{-1}
Thermal conductivity, κ_g	0.017391	W K^{-1} m^{-1}
Prandtl number, Pr	0.4024	-
Properties of the metal		
Specific heat (solid), c_{ps}	910	J kg^{-1} K^{-1}
Specific heat (liquid), c_{pl}	1178	J kg^{-1} K^{-1}
Latent on fusion, L	3.21×10^5	J kg^{-1}
Liquidus temperature, T_l	921	K
Solidus temperature, T_s	845	K
Density (@ $f = 0.5$)	2540	kg m^{-3}
Emissivity	0.12	-

The thermophysical properties of the gas are assumed to be those of argon while the thermophysical properties of the metal are generally taken as those of Al. The exceptions to this are the liquidus temperature and solidus temperature, T_l and T_s respectively, which have been obtained from the Al-Cu phase diagram. The temperature of the gas, T_g, and the effective radiative temperature of the environment, T_R, have been assumed to be equal. Moreover, all particles have been assumed to experience the same gas temperature irrespective of their diameter. The calculations have been performed at a particle temperature of $T_p = (T_l + T_s)/2 = 883$ K and on the assumption the f is linear with temperature in the melting interval, wherein $f = 0.5$ at T_p.

The results of the calculations are shown in Fig. 9, in which we show, for four different assumed gas temperatures, the differential velocity, $|v_p\text{-}v_g|$, required as a function of particles diameter, d, in order to match the measured cooling rates. On the assumption that particles of all diameters experience gas of the same temperature the minimum gas temperature is set at 600 K as below this temperature the smallest size fractions achieve the desired cooling rate, or higher, by purely radiative heat transfer. As expected, as the gas temperature increases higher differential velocities are required to achieve the measured cooling rates but in all cases the calculated differential velocities are very low, suggesting either that the particles are almost co-moving with the gas or that the gas itself has been decelerated to very low velocity. We also note that each of the four profiles calculated is relatively flat, indicating that the differential velocity between a particle and the surrounding gas is not strongly related to the particle diameter. This observation is consistent with high speed cinematography of the gas atomization process [23] in which features within the spray plume consisting of many thousands of particles, presumably covering a wide range of particle diameters, were observed to remain intact for significant periods of time, implying that the particles do indeed co-move. The inference that gas-particle velocities are so low during gas atomization may have significant implications for the understanding of the dynamics of the gas atomization process.
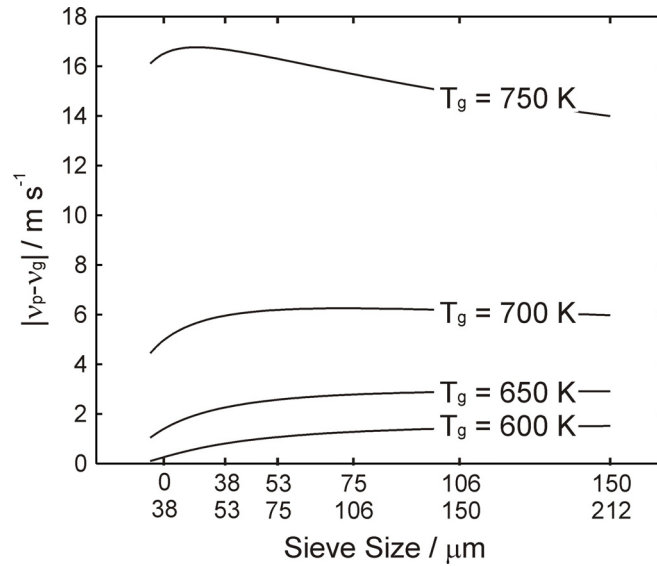
Fig. 9. Calculated differential velocity between the particles and the gas required, as a function of particle diameter, in order to achieve the measured cooling rates.

5 Summary and Conclusions

Measurement of secondary dendrite arm spacing in as-solidified, sieved, powders has been used to estimate post-recalescence cooling rates in gas atomized Al-4 wt.%Cu powder. A range of published relationships between SDAS and cooling rate have been utilised in order to estimate the uncertainty likely when converting from SDAS to cooling rate. We find that;

- There is an approximately linear relationship between SDAS and mean particle diameter. The mean SDAS varies from 7.41 μm in the 212-150 μm sieve fraction to 2.08 μm in the < 38 μm sieve fraction.
- Cooling rates have been estimated based on the relationships due to Horwath & Mondolfo [14], Eskin *et al*. [17] and Kasperovich *et al*. [18] and have been found to agree well, as have cooling rates based on a modified relationship obtained from the data of Sarreal & Abbaschian [15].
- Estimated cooling rates are found to be towards the low end of what would be expected during gas atomization, varying from ≈ 320 K s^{-1} for the 212-150 μm sieve fraction to 11000 K s^{-1} for the < 38 μm sieve fraction.
- In order for calculated cooling rates to be consistent with those determined experimentally the gas must be at a temperature close to that of the melt and the differential velocity between the gas and the melt must be low. It is likely that in this experiment the temperature difference between the gas and the melt at the point at which solidification occurred was < 200 K and that the differential velocity was $O(10$ m s$^{-1})$.

6 References

1. B. Li, X. Liang, J.C. Earthman and E.J. Lavernia: Acta Mater., 1996, vol. 44, pp. 2409–2420.
2. M. Kearns: Mater. Sci. Eng. A, 2007, vol. 375-377, pp. 120-126
3. O.P. Pandey, N.S. Mishra, C. Ramachandra, S. Lele and S.N. Ojha: Metall. Mater. Trans. A, 1994, vol. 25, pp. 2517-2523.
4. N. Zeoli, S. Gu and S. Kamnis: Int. J. Heat. Mass. Transf., 2008, vol. 51, pp. 4121–4131.
5. P. Shukla, R.K. Mandal and S.N. Ojha: Bull. Mater. Sci., 2001, vol. 24, pp. 547–554.
6. S He, Y Liu and S Guo, Rare Metal Mater. Eng., 2009, vol. 38, pp. 353-356.
7. J. Kellie, in K. O'Reilly and B. Cantor (eds.), Cooling rate and structure of commercial aluminium alloys in Solidification and Casting, Taylor & Francis 2002, pp. 271-285.
8. J. Szekely and N.J. Themelis: Rate phenomena in process metallurgy, 1972, Wiley Interscience, New York.
9. T.Z. Kattamis, J.C. Coughin and M.C. Flemings: Trans. metall. Soc. A.I.M.E., 1967, vol. 239, pp. 1504.
10. K.P. Young and D.H. Kirkwood: Metall. Trans. A, 1975, vol. 6, pp. 197-205.
11. D.H. Kirkwood: Mater. Sci. Engng, 1985, vol. 73, pp. L1-L4.
12. A.M. Mullis: Acta Mater., 1998, vol. 46, pp. 4609-4615.
13. T.F. Bower, H.D. Brody and M.C. Flemings: Trans. metall. Soc. A.I.M.E., 1966, vol. 236, pp. 624.
14. J.A. Horwath and L.F. Mondolfo: Acta Metall., 1962, vol. 10, pp. 1037-1043
15. J.A. Sarreal and G.J. Abbaschian: Metall. Trans. A, 1986, vol. 17A, 2063-73.
16. M.A. Talamantes-Silva, A. Rodríguez, J. Talamantes-Silva, S. Valtierra and R. Colás: Mater Charact., 2008, vol. 59, pp. 1434–1439.
17. D. Eskin, Q. Du, D. Ruvalcaba and L. Katgerman: Mater. Sci. Eng. A, 2005, vol. 405, pp. 1–10.
18. G. Kasperovich, T. Volkman, L. Ratke and D. Herlach: Metall. Mater. Trans. A, 2008, vol. 39, pp. 1183-1191.
19. V. Anand, A.J. Kaufman and N.J. Grant: in R. Mehrabian, B. H. Kear and M. Cohen (eds.) Rapid Solidification Processing, Principles & Technologies II, Claitor, Baton Rouge, LA, 1978, pp. 273-286.
20. I.E. Anderson, R.S. Figliola and H. Morton: Mater. Sci. Eng. A, 1991, vol. 148, pp. 101-114.
21. J. Alkemper, S. Sous, C. Stocker, and L. Ratke: J. Cryst. Growth, 1998, vol. 191, pp. 252–60
22. J. Ting, J. Connor and S. Ridder: Mater. Sci. Eng. A, 2005, vol. 390, pp. 452.
23. A.M. Mullis, N.J. Adkins, Z. Aslam, I.N. McCarthy and R.F. Cochrane: Int. J. of Powder Metall., 2008, vol. 44, pp. 55-64.
24. A.M. Mullis, I.N. McCarthy and R.F. Cochrane: J. Mater. Process. Technol., 2011, vol. 211, pp. 1471-1477.
25. R.P. Underhill, P.S. Grant, B. Cantor and D.J. Bryant: Int. J. Nonequilib. Process., 1997, vol. 10, pp. 201–216.
26. D. Bergmann, U. Fritsching and K. Bauckhage: Int. J. Therm. Sci., 2000, vol. 39, pp. 53–62.
27. M.M. Tong and D.J. Browne: J. Mater. Process. Tech., 2008, vol. 202, pp. 419–427.